0022-3565/99/2902-0917$03.00/0
THE JOURNAL OF PHARMACOLOGY AND EXPERIMENTAL THERAPEUTICS
Copyright © 1999 by The American Society for Pharmacology and Experimental Therapeutics
JPET 290:917–922, 1999

Vol. 290, No. 2
Printed in U.S.A.

Quantitative Autoradiography with Short-Lived Positron Emission Tomography Tracers: A Study on Muscarinic Acetylcholine Receptors with *N*-[^{11}C]methyl-4-piperidylbenzilate[1]

SVEN SIHVER, WIEBKE SIHVER, MATS BERGSTRÖM, A. URBAN HÖGLUND, PERNILLA SJÖBERG, BENGT LÅNGSTRÖM, and YASUYOSHI WATANABE

Department of Neuroscience, Unit of Pharmacology (S.S., W.S., Y.W.) and Department of Physiology, Unit of Comparative Medicine (U.H.), Faculty of Medicine, Uppsala University, Uppsala, Sweden; Subfemtomole Biorecognition Project, Japan Science and Technology Corporation, Toyonaka, Osaka, Japan (S.S., W.S., M.B., B.L., Y.W.); Uppsala University PET Centre, University Hospital, Uppsala, Sweden (M.B., P.S., B.L.); and Osaka Bioscience Institute, Suita-shi, Osaka, Japan (Y.W.)

Accepted for publication March 22, 1999 This paper is available online at http://www.jpet.org

ABSTRACT

The present work demonstrates quantitative autoradiography by using positron emission tomography tracers and storage phosphorimaging plates. The uptake and association of [^{11}C]*N*-methyl-4-piperidylbenzilate was measured in rat brain tissue cryosections of various thicknesses. The signal increased with increasing section thickness, but only in 10-μm-thick sections did the binding reach the steady state during a 50-min observation time. This violation of the equilibrium condition, potentially combined with perfusion limitations, leads to erroneous increased binding-site density and decreased affinity in the 25- and 50-μm-thick sections. For better imaging of receptor distribution it is reasonable to use thicker sections. For quantitative analysis of receptor-binding parameters, the specific properties of ligands at different thicknesses of cryosections need to be considered. Evidence is provided that the nonselective muscarinic antagonist *N*-methyl-4-piperidylbenzilate binds preferentially to the M_4 subtype of muscarinic acetylcholine receptors.

The autoradiography technique is well established for long-lived radiotracers and is used extensively in basic research. Since the introduction of tracers labeled with short-lived radionuclides (e.g., ^{11}C and ^{18}F with half-decay times of 20 and 110 min, respectively), the autoradiography method has come closer to in vivo positron emission tomography (PET). Ex vivo studies have been performed to assess whole-body distribution of different ^{11}C-labeled tracers in rodents (d'Argy et al., 1984, 1988). Double-tracer studies can be conducted by combining high-energy β^+- and low-energy β^--emitting radionuclides (d'Argy et al., 1984; Yanai et al., 1992). Taking advantage of the fact that high-energy β^+ particles from ^{11}C can penetrate water or biological tissues to a depth of several hundreds of micrometers, the method of spatial imaging of metabolically active brain slices has been established (Matsumura et al., 1995) and developed further for time-resolved imaging (Murata et al., 1996). Because of the rather long distance that a particle with high energy can penetrate, the imaging is not limited only to the surface of a tissue preparation but also includes deeper components of receptor-ligand interactions, which also means that ligand diffusion in the tissue comes to play a role. This fact will, in turn, affect the association and dissociation rates and the quantification of receptor binding. It was the purpose of the present work to explore some of the specific features of quantitative autoradiography when PET tracers are used.

In this study, the dependence of receptor-binding characteristics was investigated by using rat brain cryosections of different thicknesses and the muscarinic acetylcholine receptor antagonist [^{11}C]*N*-methyl-4-piperidylbenzilate ([^{11}C]NMPB). An attempt to demonstrate the receptor-subtype specificity of [^{11}C]NMPB binding also was made.

Materials and Methods

Radiochemistry and Other Chemicals. [^{11}C]Carbon dioxide was produced by the ^{14}N(p, α) ^{11}C reaction by using a nitrogen gas target and 17-megaelectron volt protons produced by an MC17 cyclotron (Scanditronix, Uppsala, Sweden) at the Uppsala University PET Center. [^{11}C]NMPB was obtained after conversion of [^{11}C]carbon dioxide to [^{11}C]methyl iodide, which then was used in an *N*-

Received for publication January 15, 1999.
[1] This work is planned to be used in Sven Sihver's Ph.D. thesis.

ABBREVIATIONS: PET, positron emission tomography; [^{11}C]NMPB, ^{11}C-labeled *N*-methyl-4-piperidylbenzilate; ROI, region of interest; M_1 to M_5, acetylcholine muscarinic receptor subtypes.

alkylation reaction of the corresponding *N*-desmethyl compound (Långström et al., 1987; Mulholland et al., 1988). The specific radioactivity ranged from 41.4 to 141.3 GBq/μmol at the end of the synthesis.

Atropine sulfate and pirenzepine were obtained from Research Biochemicals International (Natick, MA). Green mamba (*Dendroaspis angusticeps*) venom (0.5 g) was purchased freeze-dried from Miami Serpentarium Laboratories (Miami, FL), and reconstituted venom was filtered by use of Centriprep-3 (Millipore, Bedford, MA) filter tubes and centrifuged at 3000 rpm in a Midispin centrifuge (LKB, Gaithersburg, MD) until equilibrium had been achieved. The supernatant was resuspended in ammonium acetate buffer (30 mM, pH 6.8) to 15 ml and centrifuged again. This procedure was repeated three times to rid the crude venom of low-molecular-weight substances that might interfere with the autoradiography. After the last centrifugation, the supernatant was resuspended in ammonium acetate buffer to a total volume of 15 ml. The protein concentration was determined spectrophotometrically at 562 nm by using the BCA (bicinchoninic acid) Protein Assay (Pierce, Rockford, IL) with buffer as a reference (Smith et al., 1985). The venom finally was divided into 1-ml aliquots and kept in a freezer at −70°C until use.

Animals. Male Sprague-Dawley rats weighing 200 to 300 g were used. They were kept at a constant temperature (20°C) and humidity (50%) with a constant light/dark cycle, with light on from 7:00 AM to 7:00 PM, and given free access to laboratory animal chow and water. The animals were anesthetized with carbon dioxide and decapitated. Thereafter, the brains were quickly removed and stored at −70°C until use. The animal studies were approved by the local Animal Ethics Committee of Uppsala (registration no. C 174/93).

[^{11}C]NMPB Autoradiography. The in vitro autoradiography was performed in general as discussed by Kuhar (1985). Coronal or sagittal sections of different thicknesses (10–125 μm) were cut with a cryostat microtome (SLEE Technik GmbH, Mainz, Germany), mounted on gelatin-coated glass slides, dried at room temperature, and stored at −20°C until they were to be used for experiments within 2 weeks. For treating the sections, the conditions described by Kloog et al. (1979) were used with minor modifications. Briefly, the sections were preincubated in modified Krebs-Henseleit buffer containing 25 mM Tris-HCl, 118 mM NaCl, 4.69 mM KCl, 1.9 mM $CaCl_2$, 0.54 mM $MgCl_2$, 1 mM NaH_2PO_4, and 11.1 mM glucose (pH 7.4) for 40 min at 37°C. To define the total binding, we incubated these sections at different concentrations of [^{11}C]NMPB in the same buffer at 37°C for 50 min. Nonspecific binding was determined in adjacent sections incubated in the presence of 10 μM atropine. After the incubation, the sections were washed twice for 5 min each time with the incubation buffer and subsequently dipped into distilled water and dried under a stream of warm air (40°C). The sections were exposed for 40 min to recyclable storage phosphorimaging plates, which are sensitive to positrons (β^+). The imaging plates were scanned with a laser beam in the image-reading unit of the PhosphorImager (model 400S, Molecular Dynamics, Sunnyvale, CA). Scanning operations and image display and analysis were performed by the software ImageQuant (Molecular Dynamics).

The signal dependence on slice thickness was determined in cryosections of 10- to 125-μm thickness. The incubation procedure was performed as described above using [^{11}C]NMPB concentrations of 0.5 and 5.0 nM. The association kinetics were determined using 10-, 25-, and 50-μm-thick cryosections. The incubation of the samples with 1 nM [^{11}C]NMPB was started at the longest time point (50-min) and terminated simultaneously in all samples at time zero. In saturation experiments, 10-, 25-, and 50-μm-thick cryosections were incubated with various concentrations of [^{11}C]NMPB (0.05–12.8 nM) at 37°C for 50 min. For determination of receptor subtype specificity of [^{11}C]NMPB, the 10-μm-thick sections were incubated in the presence of various concentrations of pirenzepine (0.3–3000 nM), which is a predominantly M_1 muscarinic receptor subtype 1 specific antagonist, or crude venom of the green mamba (30 μg of protein/ml), which is known to contain M_1 and M_4 receptor subtype-specific antagonist toxins (Jerusalinsky and Harvey, 1994; Jolkkonen et al., 1994).

For quantification, individual calibration standards were prepared for each set of brain sections exposed to the same imaging plate. The standard was a 20-μl drop of [^{11}C]NMPB solution of known concentration placed on a thin, absorbent paper (BenchGuard; Bibby Sterlin Ltd., Staffordshire, UK) and exposed simultaneously with the brain sections. Knowing the concentration and volume of the standard sample, we calculated the amount of substance expressed in fmol. The total counts over the standard, measured by the phosphorimaging system, allowed the calculation of a calibration factor in counts per femtomole. The signal measured for a region of interest (ROI) in a structure of a brain slice was given as average counts per pixel. Knowing the pixel size, we recalculated the value to counts per square millimeter and, using the calibration factor, converted it further to femtomoles per square millimeter (and femtomoles per cubic millimeter). Before this calculation, the average counts per pixel of the background area close to the brain slices was subtracted from the average counts of the ROI.

Results

The influence of the cryosection thickness on the strength of the phosphorimager signal was investigated in a thickness range from 10 to 125 μm. The slice thickness at which the signal reached the maximum was dependent on the concentration of the tracer (Fig. 1). In the case of 0.5 nM [^{11}C]NMPB, the maximal signal was reached at 25 μm, and, with 5 nM [^{11}C]NMPB, it was reached at a slice thickness of 50 μm. The maximal signal level differed by 10-fold between these two concentrations.

To determine the time for reaching the apparent equilibrium, we selected a 1-nM incubation concentration of [^{11}C]NMPB. The kinetics were evaluated in cryosections of 10-, 25-, and 50-μm thickness. Equilibrium was reached only in the case of 10-μm-thick sections, with more than 90% of the steady-state level reached within 30 min. The association

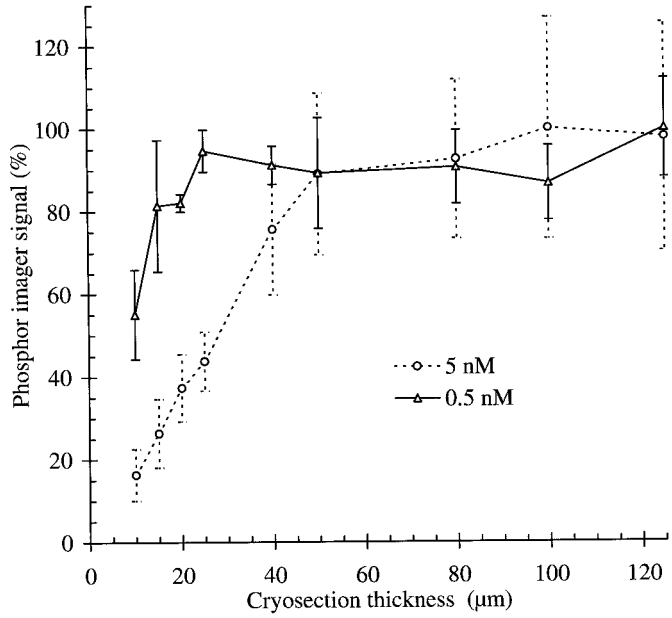

Fig. 1. Phosphorimager signals were normalized to the highest value and plotted against the thickness of rat forebrain cryosections. Two concentrations of [^{11}C]NMPB were used: 5 nM (○ and dotted line) and 0.5 nM (△ and continuous line). There was a 10-fold difference in absolute values between these two concentrations. The graphs represent the mean of four separate experiments with S.E.M. (error bars).

$T_{1/2}$ was 9 min (Fig. 2). In 25- and 50-μm-thick sections, a continuous uptake of [^{11}C]NMPB was observed throughout the incubation period.

The concentration dependence of specific [^{11}C]NMPB binding was studied in the cerebral cortex and caudate putamen (striatum) in 10-, 25-, and 50-μm-thick sections. The specific binding in cortex and striatum (Fig. 3, A and C) appeared to be saturable over a concentration range of 0.05 to 12.8 nM [^{11}C]NMPB. The Scatchard plots of the saturation data for 10-μm-thick sections were linear, suggesting a homogeneous population of binding sites in both regions examined (Fig. 3, B and D). Table 2 shows that the binding constants (K_D and B_{max}) in the two investigated brain regions depended on the thickness of the sections. B_{max} expressed in femtomoles per cubic millimeter was slightly higher in the striatum than in the cortex, but the increase with increasing section thickness was not statistically significant. K_D was higher in thicker sections.

Figure 4 shows the autoradiograms of the [^{11}C]NMPB binding (0.8 nM) in coronal (Fig. 4, columns A and C) and sagittal (Fig. 4, columns B and D) 10-, 25-, and 50-μm-thick sections of rat brain. With a pseudocolor scale of the images (Fig. 4, columns A and B) adjusted to the highest phosphorimager signal in each section thickness, a more defined and clear image, less disturbed by the background noise, was observed in the thicker sections. A significant increase in signal related to section thickness was obvious when the same scale (Fig. 4, columns C and D) was applied. The highest [^{11}C]NMPB-binding density was found in the striatum, followed by hippocampus and cortex, and it was much lower in other regions of the brain.

Although the Scatchard plots suggest that NMPB binds to a uniform population of receptors, a competition study was performed to investigate the subtype specificity of [^{11}C]NMPB. In five displacement experiments, pirenzepine and crude venom of the green mamba were used. Pirenzepine at 30, 300, and 3000 nM displaced the total binding of [^{11}C]NMPB by 15, 40, and 60%, respectively, in cortex and striatum, and by 0, 16, and 40%, respectively, in the spinal cord in 10-μm-thick sections (Fig. 5). The crude venom of the green mamba (30 μg of protein/ml) displaced the total binding of the [^{11}C]NMPB by 53, 60, and 13% in cortex, striatum, and spinal cord, respectively, in 10-μm-thick sections (Fig. 6).

The nonspecific binding measured in the presence of 10 μM atropine ranged from 5 to 10% of the total binding in all experiments.

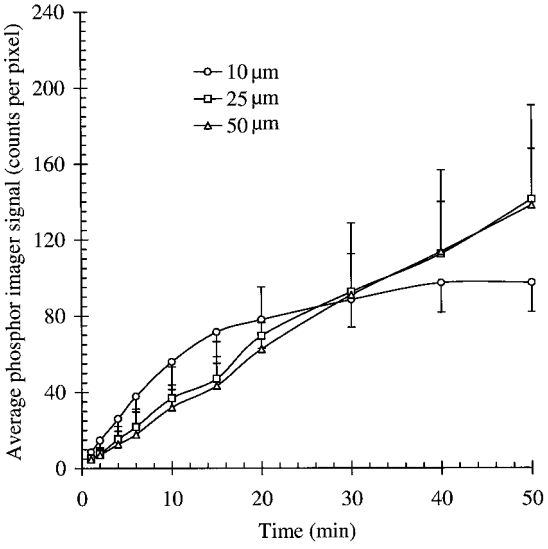

Fig. 2. Association kinetics related to slice thickness. ○, 10-μm-thick sections; □, 25-μm-thick sections; and △, 50-μm-thick sections. The average phosphorimaging signal (counts per pixel) in the ROIs is plotted against the association time. The graphs shows the mean of four separate experiments with S.E.M. (error bars).

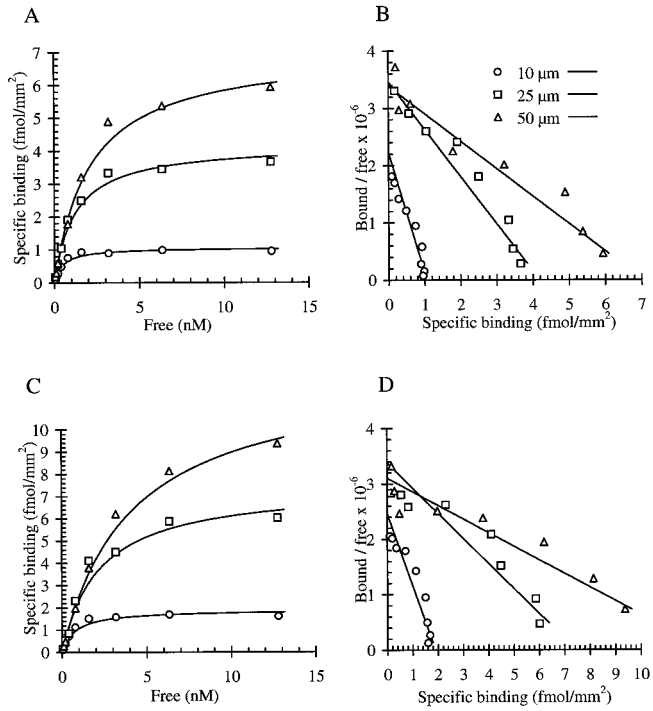

Fig. 3. Saturation curves (A and C) and Scatchard plots (B and D) of specific [^{11}C]NMPB binding in the cortex (A and B) and in the striatum (C and D) of rat brain sections of 10- (○), 25- (□), and 50-μm (△) thickness. The graphs show the results of a single representative experiment. The average values for K_D and B_{max} from five experiments are shown in Table 2.

Discussion

The study of binding characteristics of short-lived radionuclide-labeled ligands in vitro is of increasing interest as a means of characterizing the tracer before application in vivo to obtain complementary information needed to clarify in vivo distribution or to explore new applications. The use of PET tracers in vitro may also be beneficial in view of their easy application to the phosphorimaging system and, thus, the fast receiving of results (d'Argy et al., 1988). For the application of PET tracers to autoradiography, the phosphorimaging technique, different properties of the tracers, and the measurement system have to be considered, as illustrated in the present work.

The binding properties of the ^{11}C-labeled muscarinic acetylcholine receptor ligand [^{11}C]NMPB were compared for different section thicknesses in frozen-section autoradiography. Images with stronger signals were obtained with thicker cryosections. The signal linearly increased from 10 to 25 μm (in the case of 0.5 nM [^{11}C]NMPB) or to 50 μm (in the case of 5 nM [^{11}C]NMPB). A similar linear relation between the thickness of sections from 5 to 14 μm was demonstrated for a ^{125}I-labeled tracer (Tang et al., 1995). This shows that in

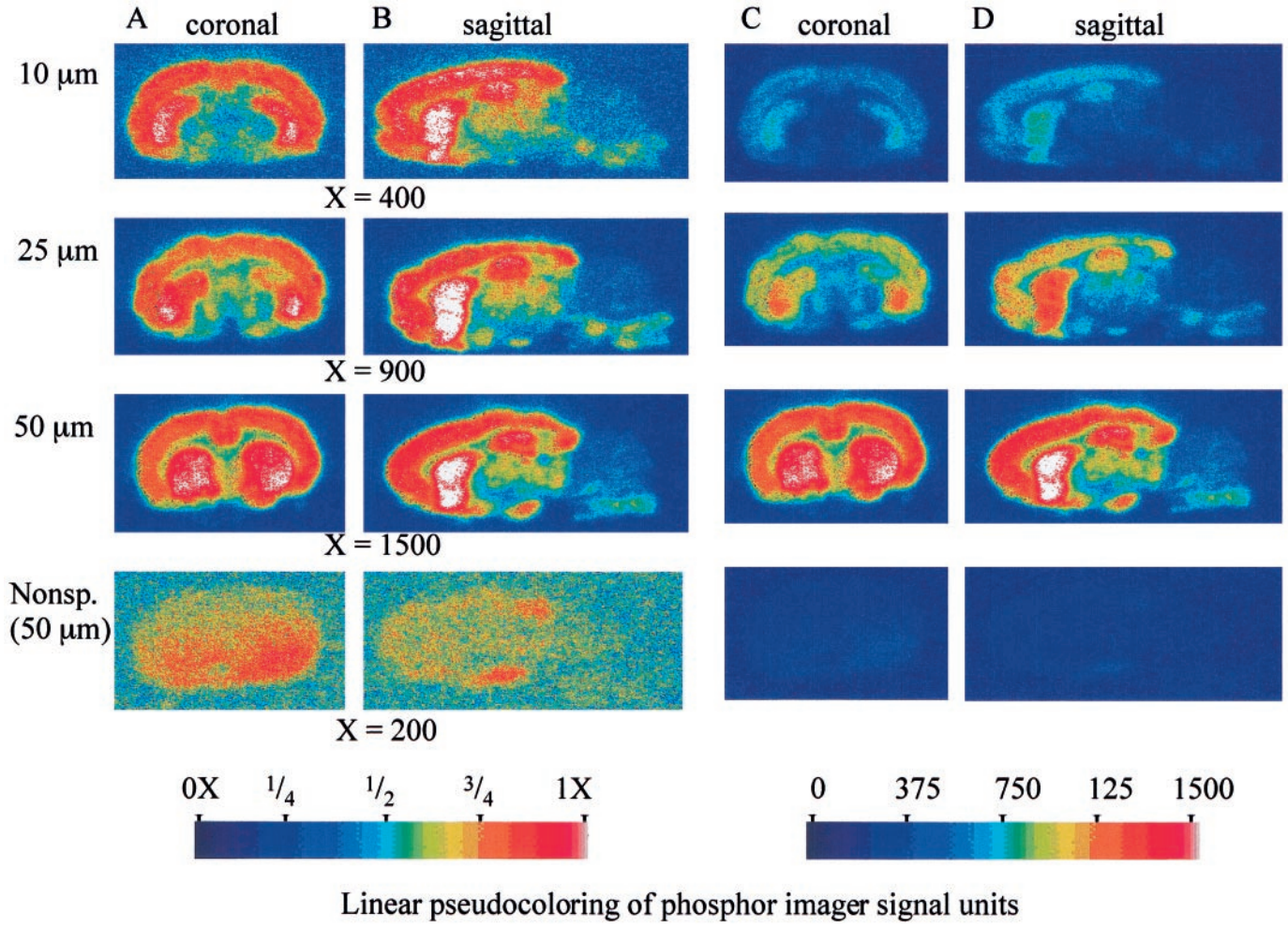

Fig. 4. Autoradiographic images of [^{11}C]NMPB binding (0.8 nM) in coronal-columns (A and C) and sagittal-columns (B and D) cryosections of the rat brain. The images were visualized by exposing the rat brain slices for 40 min to an imaging plate sensitive to positrons (β^+). Top, total binding images of 10-, 25-, and 50-μm-thick sections are shown. Bottom, nonspecific binding in 50-μm-thick sections obtained in the presence of 10 μM atropine. A and B, images were pseudocolored with a scale adjusted to the highest signal for each section thickness. C and D, same scale with the same highest value was applied to all images obtained from 10-, 25-, and 50-μm-thick cryosections.

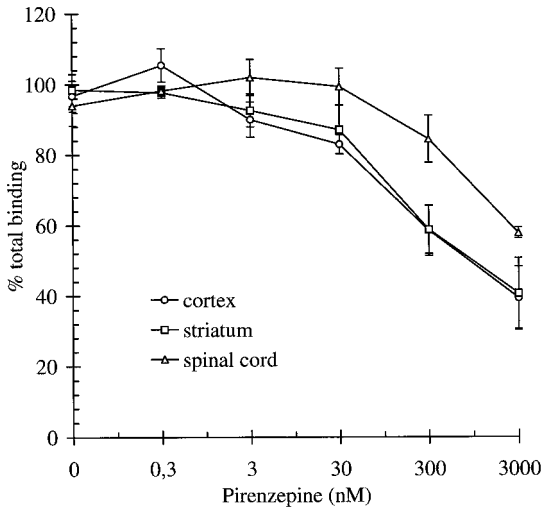

Fig. 5. Displacement of the [^{11}C]NMPB binding (0.8 nM) by different concentrations of pirenzepine in rat cerebral cortex (○), striatum (□), and spinal cord (△) of 10-μm-thick cryosections. The curves represent five separate experiments with S.E.M. (error bars).

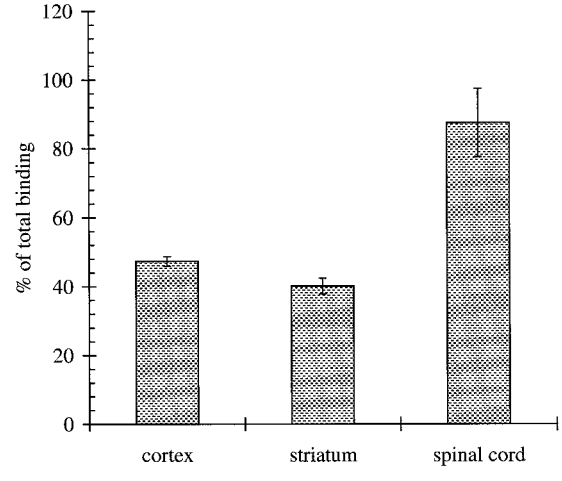

Fig. 6. The binding of 0.8 nM [^{11}C]NMPB in the cerebral cortex, striatum, and spinal cord of 10-μm-thick cryosections of rat brain in the presence of 30 μg of protein/ml of crude venom of the green mamba. The binding is shown as a percentage of total binding obtained by incubating corresponding sections without the venom. The graph shows the mean values of four separate experiments with S.E.M. (error bars).

TABLE 1
Successive steps in the quantification of receptor binding in quantitative frozen-section autoradiography with ^{11}C-labeled tracers

Production of ^{11}C-labeled radiotracer and evaluation of its concentration (μg/ml)
↓
Standard dilution of the ^{11}C-labeled tracer with known concentration (nM)
↓
Preincubation, incubation, washing, and drying of the sections
↓
Preparation of the standard: a 20-μl drop of the standard dilution on a thin, absorbent paper on a non-slip-coated side (e.g., BenchGuard)
↓
Exposing the cryosections together with the standard to a phosphorimaging plate (One standard is necessary for each plate)
↓
Drawing a circular ROI over the image of the standard drop and computing the sum of all pixel values in this ROI; calculation of the calibration factor in counts/fmol of ^{11}C-labeled tracer
↓
Converting the average counts/pixel in ROIs delineated in the images of the cryosections to fmol/area (mm^2) or volume (mm^3) using the calibration factor and pixel size

frozen-section autoradiography with PET tracers, it is possible to achieve a better signal and, hence, a better image by increasing the thickness of the slice. This is not the case with ^{3}H-labeled tracers, where the penetration depth of the β^- particles constitutes a limitation. Loss of resolution because of increased scattering of β^+ particles in the case of 50-μm-thick sections if compared with 10- or 25-μm-thick sections is only minimal because the spatial resolution (expressed as full width of half-maximum) of storage phosphorimaging plates, when working with ^{11}C-labeled tracers, is around 600 μm (Sihver et al., 1997).

Binding equilibrium was possible to reach only in the case of 10-μm-thick sections (Fig. 2). In 25- and 50-μm-thick ones, the association and uptake process continued up to the end of the follow-up time, which, because of the fast physical decay of the ^{11}C radioactivity close to the background radiation, was limited to 50 min. In 200-μm-thick living brain slices incubated with 2 nM [^{11}C]NMPB, the binding equilibrium was reached after 100 and 130 min in rat cortex and striatum, respectively (Murata et al., 1998). To evaluate binding at equilibrium in thicker slices and to determine the dissociation kinetics thus is practically difficult. The association perhaps would be faster and the time for the tracer binding to reach the apparent steady state would be shorter if a higher concentration of [^{11}C]NMPB would have been used. Because lower concentrations of radioligand take longer to equilibrate, the low concentration of radioligand was used for measuring how long it takes the incubation to reach equilibrium. The nonequilibrium effect of premature termination of the incubation is more prominent in low than in high concentrations, therefore it appears a shift from off-rate-limited to on-rate-limited kinetics in the low concentration range. Performing a Scatchard analysis of such data leads to overestimation of both K_D and B_{max} (Hulme and Birdsall, 1993). However, there is the reason to believe also that such possible factors as tracer diffusion within the tissue and its local concentration and possible local depletion and modification by local nonspecific binding have their role to play in differences in ligand-binding kinetics. That is supported by the observations of 8-fold-higher K_D for [^{3}H]quinuclidinyl benzilate (Gilbert et al., 1979) and 20-fold-higher K_D for [^{11}C]NMPB (Murata et al., 1998) for native brain slices than for homogenates, or the 3- to 10-fold difference in K_D for raclopride when comparing the binding between human brain homogenates (Hall et al., 1990) and human brain in vivo by use of the PET technique (Farde et al., 1995).

Because the storage phosphorimaging plates have superior sensitivity and a linear response over a wide radioactivity range, it is possible to accurately record the PET tracer's radioactivity at a low concentration range with a sufficient signal-to-noise ratio (Sihver et al., 1997). Because of the linearity, it is sufficient to use one concentration as a standard for calibration, and it should be exposed at the same time as the brain sections. Previously, we confirmed that the suggested procedure with a 20-μl drop of tracer solution on an absorbent paper as a standard has good accuracy in comparison with the measurement of 1 ml of the same solution with a gamma counter (data not shown). With PET-tracer autoradiography, it is a straightforward procedure to measure specific binding expressed as femtomoles per square millimeter (Table 1).

The present study has demonstrated that the K_D of [^{11}C]NMPB is dependent on the slice thickness, indicating that factors other than ligand receptor interactions are involved. The K_D values for [^{3}H]NMPB in cortex and striatum homogenates of mouse brain were 0.41 ± 0.03 and 0.38 ± 0.01 nM, respectively, and there appeared to be more binding sites in the striatum than in the cortex (Kloog et al., 1979), which is in good agreement with our results with 10-μm-thick sections. There was a loss in tracer affinity in thicker

TABLE 2
Scatchard plot analysis of saturation data of [^{11}C]NMPB binding in autoradiography of frozen sections of different thicknesses

	10 μm		25 μm		50 μm	
	Cortex	Striatum	Cortex	Striatum	Cortex	Striatum
K_D (nM)	0.49 (0.10)	0.69 (0.15)	1.12 (0.16)	1.49 (0.31)	1.93 (0.21)	3.13 (0.44)
B_{max} (fmol/mm^2)	1.01 (0.18)	1.73 (0.37)	3.07 (0.46)	3.71 (1.26)	8.68 (2.43)	14.13 (4.24)
B_{max} (fmol/mm^3)	101 (18)	173 (37)	122.8 (18.4)	148.4 (50.4)	173.6 (48.6)	282.6 (84.8)

The data represented are the mean (±S.E.M.) of at least four independent experiments.

sections. The average ratio between the binding capacity in cortex and striatum in sections of the three different thicknesses was 0.66 (with S.E.M. ± 0.08), which means that the relative pattern of binding-site distribution was retained even if equilibrium was not reached in the thicker sections. The evaluation of quantitative binding parameters in this type of frozen-section autoradiography must be interpreted with caution, because the results might be influenced by such an experimental variable as thickness of the cryosections.

The general binding pattern of the [^{11}C]NMPB autoradiograms is in good agreement with the binding distribution of [^{3}H]NMPB in mouse brain homogenate preparations (Kloog et al., 1979) and similar to the binding pattern of the [^{3}H]quinuclidinyl benzilate autoradiography in the rat brain (Cortes and Palacios, 1986; Biegon et al., 1988).

When a calculation was made from the displacement of ligand from muscarinic acetylcholine receptors by pirenzepine, it was found that 30 nM pirenzepine displaced a major part of the available M_1 (83%) and that 300 nM pirenzepine displaced M_1 (98%) and M_4 (68%) muscarinic receptor subtypes (Höglund and Baghdoyan, 1997). That 30 nM pirenzepine did not displace the [^{11}C]NMPB binding in the spinal cord but displaced about 15% of total [^{11}C]NMPB binding in the cortex and striatum suggested that the M_1 subtype is not present in the spinal cord, which is consistent with previous findings (Höglund and Baghdoyan, 1997). Only 15% of the total [^{11}C]NMPB binding in the cortex and striatum appeared to be accounted for by the M_1 subtype, which is abundant in these regions (Flynn et al., 1998). Pirenzepine at 300 nM displaced on average 16% of the total [^{11}C]NMPB binding in the spinal cord, apparently because of a block of a majority of the M_4 subtype. This suggestion is strengthened by the observation that 30 μg of protein/ml of crude green mamba venom, which is known at this concentration to bind preferentially to M_1 and M_4 subtypes (Jolkkonen et al., 1994; Flynn et al., 1998), displaced 13% of the total [^{11}C]NMPB binding in the spinal cord. Because the mamba venom displaced approximately half of the [^{11}C]NMPB binding in the cortex and striatum and the effect of 300 nM but not that of 30 nM pirenzepine was in the same range, we conclude that [^{11}C]NMPB binds preferentially to the M_4 subtype of muscarinic acetylcholine receptor. A concentration of 3 μM pirenzepine displaced the [^{11}C]NMPB binding further, indicating an additional binding of [^{11}C]NMPB to M_2, M_3, and M_5 subtypes of the muscarinic acetylcholine receptor.

Conclusions

Quantitative autoradiography can be performed with short-lived PET tracers, but, as established in this work, it is necessary to consider that the time to reach equilibrium is dependent on the slice thickness. The use of thicker sections gives a better signal and, thus, better resolved images but perhaps at the expense of deteriorated quantification. On the other hand, in the case of equilibrium conditions, the long distance that the high-energy β^+ particles from ^{11}C penetrate in biological tissue gives an advantage in quantifying the binding in small structures, which theoretically could be measured within a single cryosection instead of in many thin, consecutive sections. The storage phosphorimaging plate is an ideal tool for the generation of images because of its high sensitivity and linear response over a large concentration range.

[^{11}C]NMPB is nonselective with respect to subtypes of muscarinic receptors. Depending on the experimental conditions, different subtypes may be accentuated, but our data suggest that [^{11}C]NMPB binds preferentially to the M_4 subtype.

References

Biegon A, Duvdevani R, Greenberger V and Segal M (1988) Aging and brain cholinergic muscarinic receptors: An autoradiographic study in the rat. *J Neurochem* **51:**1381–1385.

Cortes R and Palacios JM (1986) Muscarinic cholinergic receptor subtypes in the rat brain. I. Quantitative autoradiographic studies. *Brain Res* **362:**227–238.

d'Argy R, Paul R, Frankenberg L, Stålnacke C-G, Lundqvist H, Kangas L, Halldin C, Någren K, Roeda D, Haaparanta M, Solin O and Långström B (1988) Comparative double-tracer whole-body autoradiography: Uptake of ^{11}C-, ^{18}F- and ^{3}H-labeled compounds in rat tumours. *Int J Radiat Appl Instrum Part B* **15:**577–585.

d'Argy R, Ullberg S, Stålnacke C-G and Långström B (1984) Whole-body autoradiography using ^{11}C with double-tracer applications. *Int J Appl Radiat Isot* **35:**129–134.

Farde L, Hall H, Pauli S and Halldin C (1995) Variability in D2-dopamine receptor density and affinity: A PET study with [^{11}C]raclopride in man. *Synapse* **20:**200–208.

Flynn DD, Reever CM and Ferrari-DiLeo G (1997) Pharmacological strategies to selectively label and localize muscarinic receptor subtypes. *Drug Dev Res* **40:**104–116.

Gilbert RFT, Hanley MR and Iversen LL (1979) [^{3}H]-Quinuclidinyl benzilate binding to muscarinic receptors in rat brain: Comparison of results from intact brain slices and homogenates. *Br J Pharmacol* **65:**451–456.

Hall H, Wedel I, Halldin C, Kopp J and Farde L (1990) Comparison of the in vitro receptor binding properties of N-[^{3}H]methylspiperone and [^{3}H]raclopride to rat and human brain membranes. *J Neurochem* **55:**2048–2057.

Höglund AU and Baghdoyan HA (1997) M2, M3 and M4 but not M1, muscarinic receptor subtypes are present in rat spinal cord. *J Pharmacol Exp Ther* **281:**470–477.

Hulme EC and Birdsall NJM (1993) Strategy and tactics in receptor-binding studies, in *Receptor-Ligand Interactions. A Practical Approach* (Hulme EC ed) pp 63–176, Oxford University Press, Oxford.

Jerusalinsky D and Harvey AL (1994) Toxins from mamba venoms: Small proteins with selectivities for different subtypes of muscarinic acetylcholine receptors. *Trends Pharmacol Sci* **15:**424–430.

Jolkkonen M, van Giersbergen PLM, Hellman U, Wernstedt C and Karlsson E (1994) A toxin from the green mamba *Dendroaspis angusticeps:* Amino acid sequence and selectivity for muscarinic m4 receptors. *FEBS Lett* **352:**91–94.

Kloog Y, Egozi Y and Sokolovsky M (1979) Characterization of muscarinic acetylcholine receptors from mouse brain: Evidence for regional heterogeneity and isomerization. *Mol Pharmacol* **15**:545–558.

Kuhar MJ (1985) Receptor localization with the microscope, in *Neurotransmitter Receptor Binding* (Yamamura HI, Enna SJ and Kuhar MJ eds) pp 153–176, Raven Press, New York.

Långström B, Antoni G, Halldin C, Gullberg P, Malmborg P, Någren K, Rimland A and Svärd H (1987) Synthesis of L- and D-(methyl-^{11}C)methionine. *J Nucl Med* **28:**1037–1040.

Matsumura K, Bergström M, Onoe H, Takechi H, Westerberg G, Antoni G, Bjurling P, Jacobson GB, Långström B and Watanabe Y (1995) In vitro positron emission tomography (PET): Use of positron emission tracers in functional imaging in living brain slices. *Neurosci Res* **22:**219–229.

Mulholland GK, Jewett DW, Otto CA, Kilbourn MR, Sherman PS and Kuhl DE (1988) Synthesis and regional brain distribution of [C-11]*N*-methyl-4-piperidyl benzilate ([C-11]NMPB) in the rat. *J Nucl Med* **29:**768.

Murata T, Matsumura K, Onoe H, Bergström M, Takechi H, Sihver S, Sihver W, Neu H, Andersson Y, Ögren M, Fast K-J, Långström B and Watanabe Y (1996) Receptor imaging technique with ^{11}C-labeled receptor ligands in living brain slices: Its application to time-resolved imaging and saturation analysis of benzodiazepine receptor using [^{11}C]Ro15–1788. *Neurosci Res* **25:**145–154.

Murata T, Matsumura K, Sihver S, Onoe H, Bergström M, Sihver W, Yonekura Y, Långström B and Watanabe Y (1998) Triazolam-induced modulation of muscarinic acetylcholine receptor in living brain slices as revealed by a new positron-based imaging technique. *J Neural Transm* **105:**1117–1127.

Sihver W, Sihver S, Bergström M, Murata T, Matsumura K, Onoe H, Andersson Y, Bjurling P, Fasth KJ, Westerberg G, Ögren M, Jacobson G, Lundqvist H, Oreland L, Watanabe Y and Långström B (1997) Methodological aspects for in vitro characterization of receptor binding using ^{11}C-labeled receptor ligands: A detailed study with the benzodiazepine receptor antagonist [^{11}C]Ro 15–1788. *Nucl Med Biol* **24:**723–731.

Smith PK, Krohn RI, Hermanson GT, Mallia AK, Gartner FH, Provenzano MD, Fujimoto EK, Goeke NM, Olson BJ and Klenk DC (1985) Measurement of protein using bicinchoninic acid. *Anal Biochem* **150:**76–85.

Tang C, Biemond I and Lamers CBHW (1995) Localisation and quantification of cholecystocinin receptors in rat brain with storage phosphor autoradiography. *BioTechniques* **18:**886–889.

Yanai K, Ryu JH, Watanabe T, Iwata R and Ido T (1992) Receptor autoradiography with ^{11}C and ^{3}H-labeled ligands visualized by imaging plates. *NeuroReport* **3:**961–964.

Send reprint requests to: Mats Bergström, UAS, Uppsala University PET Centre, S-75185 Uppsala, Sweden. E-mail: mats.bergstrom@pet.uu.se